

Observing the deformation of nuclei with relativistic nuclear collisions

Giuliano Giacalone¹

¹*Institut de physique théorique, Université Paris Saclay, CNRS, CEA, F-91191 Gif-sur-Yvette, France*

I show that particle collider experiments on relativistic nuclear collisions can serve as direct probes of the deformation of the colliding nuclear species. I argue that collision events presenting very large multiplicities of particles and very small values of the average transverse momentum of the emitted hadrons probe collision geometries in which the nuclear ellipsoids fully overlap along their longer side. By looking at these events one selects interaction regions whose elliptic anisotropy is determined by the deformed nuclear shape, which becomes accessible experimentally through the measurement of the elliptic flow of outgoing hadrons.

INTRODUCTION

I present a method to access experimentally the deformation of the ground state of nuclei using relativistic nuclear collisions performed at the BNL Relativistic Heavy Ion Collider (RHIC) and at the CERN Large Hadron Collider (LHC).

In these experiments, nuclei are smashed at very high energy to produce the quark-gluon plasma (QGP) [1], the high-temperature state of strong-interaction matter. The little droplet of QGP created in a nuclear collision exists for a very short time before decoupling into thousands of particles, and can not be observed directly. Its presence can only be inferred by looking at specific signatures (e.g., long-range correlations and anisotropies [2]) which it imprints on the distribution of particles emitted to the final state.

Surprisingly enough, the final states of nucleus-nucleus collisions carry information about the shape of the colliding nuclei. The reason is that the QGP is a hydrodynamic medium [3], whose dynamics is governed by pressure-gradient forces:

$$F = -\nabla P, \quad (1)$$

where F is the force per unit volume, and ∇P is the pressure gradient. The QGP is essentially at rest when it is created, so that the pressure gradients and the subsequent flow of the medium are determined by the geometry of the system at the initial condition of the hydrodynamic expansion. The global features of the geometry of the system in turn emerge from the way the two nuclei overlap in the interaction. For a collision occurring at zero impact parameter, the geometry of overlap is determined by the spatial orientations of the nuclei, which are in general non-spherical objects (see Fig. 1).

The orientations of the colliding nuclei are random, and induce fluctuations in the geometry of overlap. These fluctuations leave distinct signatures in the observables that probe the hydrodynamic flow of the QGP in nucleus-nucleus analyses [4–6]. However, experimentally one does not know how to select collision events in which the orientations of the nuclei are fixed, so that observables reconstructed from the final-state particles are always the

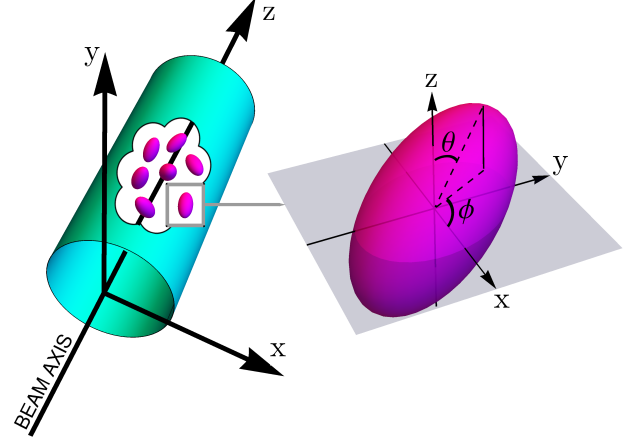


FIG. 1. A bunch of deformed nuclei accelerated in a beam pipe. The beam axis runs along the z axis. Individually, each nucleus has a random orientation in space, determined by a polar angle, θ , and an azimuthal angle, ϕ .

outcome of an average over orientations. For this reason, current analyses of nucleus-nucleus data are unable to put constraints the structure of the colliding species.

Here I point out a simple application of Eq. (1) that permits to select nucleus-nucleus events in which the orientation of the nuclei is fixed. This gives access to collision geometries that follow very closely the shape of the colliding bodies. As I will demonstrate, in such configurations the flow of emitted particles becomes a direct measure of the deformation of the nuclei.

FREEZING NUCLEAR ORIENTATIONS

Consider an axially-symmetric nucleus with a static quadrupole deformation. Its density of matter can be written as

$$\rho(\mathbf{x}', z') = \frac{\rho_0}{1 + \exp \left\{ \frac{1}{a} \left[\sqrt{|\mathbf{x}'|^2 + z'^2} - R(1 + \beta Y_{20}) \right] \right\}}, \quad (2)$$

where z' is the axis of the nucleus, \mathbf{x}' is a coordinate in the plane orthogonal to z' , and spherical symmetry is broken by the spherical harmonic that carries a dependence on the angle Θ between \mathbf{x}' and z' , $Y_{20} = \sqrt{\frac{5}{16\pi}}(3\cos^2\Theta - 1)$. The quantity a is the diffusiveness of the nucleus, R is its average radius, and ρ_0 is the density of nuclear matter. The magnitude of the quadrupole deformation is controlled by the parameter β , which quantifies the eccentricity of the nuclear ellipsoid. A nucleus is spherical for $\beta = 0$, prolate for $\beta > 0$, and oblate for $\beta < 0$.

Let me inject such a nucleus in the beam pipe of a particle collider. The laboratory frame is defined by a the beam axis, z , and the plane orthogonal to it, \mathbf{x} , the so-called *transverse* plane. As illustrated in Fig. 1, each nucleus in the beam pipe is randomly oriented in space, so that the frames (z', \mathbf{x}') and (z, \mathbf{x}) differ in general by polar tilt, θ , and by an azimuthal spin, ϕ . The geometry of the collision of two nuclei, say A and B, in the laboratory frame is therefore determined by two polar tilts, θ_A and θ_B , and two azimuthal spins, ϕ_A and ϕ_B [7].

Equation (1) and the dimensional analysis imply that

$$F \propto \frac{1}{R}, \quad (3)$$

where R is the transverse size of the system¹. In general, a fluid of initial size R_1 undergoes a larger acceleration than a fluid of initial size R_2 if $R_1 < R_2$, and if the two fluids contain the same total entropy. In the context of nuclear collisions, one can select two QGPs containing the same total entropy by looking at two events presenting the same multiplicity (the same number of particles emitted to the final state), since total entropy is to a good approximation conserved during the hydrodynamic phase. The QGP presenting the smaller value of R at the initial condition undergoes, then, a more explosive expansion, that builds momentum more rapidly. Its fluid cells reach the decoupling hypersurface with a larger velocity, producing particles that carry more transverse momentum, $p_t = \sqrt{p_x^2 + p_y^2}$, to the final state [9]. This argument is confirmed by hydrodynamic simulations [10, 11], where the initial size of the system, R , and the average transverse momentum of the produced hadrons, \bar{p}_t , at fixed multiplicity are anti-correlated:

$$\text{smaller } R \Rightarrow \text{larger } \bar{p}_t. \quad (4)$$

Let us have a look at Fig. 2. Body-body collisions present $\theta_A = \theta_B = \frac{\pi}{2}$, while tip-tip collisions present

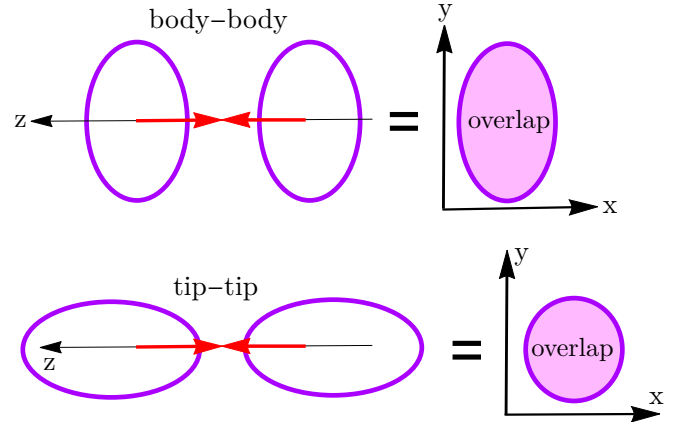


FIG. 2. Tip-tip and body-body collisions of non-spherical nuclei along with the corresponding transverse areas of overlap at fixed z .

$\theta_A = \theta_B = 0$. The area of overlap is naturally larger in body-body collisions. If one takes R as the rms radius of the system weighted by the entropy density profile, $s(\mathbf{x})$,

$$R^2 = \frac{\int_{\mathbf{x}} |\mathbf{x}|^2 s(\mathbf{x})}{\int_{\mathbf{x}} s(\mathbf{x})} \quad (5)$$

then, at fixed multiplicity, body-body collisions present the larger values of R , and, by virtue of Eq. (4), smaller values of \bar{p}_t than tip-tip collisions. The crucial implication of this result is that it provides an experimental method to select the orientation of the colliding nuclei. First, choose events at fixed multiplicity (possibly large, to reduce the role of impact parameter). Then, sort events according to the \bar{p}_t of the produced hadrons. Events with abnormally low values of \bar{p}_t correspond to fully overlapping body-body collisions.

I perform an explicit application of this selection procedure in model simulations of the collision process. I use the phenomenologically-successful TRENTo model of initial conditions [12]. In this model, the profile of entropy density created in the interaction of nuclei A and B behaves like $s(\mathbf{x}) \propto \sqrt{T_A(\mathbf{x} + \mathbf{b}/2)T_B(\mathbf{x} - \mathbf{b}/2)}$, where $T_{A/B}(\mathbf{x})$ is a Lorentz-boosted matter density, given by the integral of Eq. (2) along the beam axis, z , and \mathbf{b} is the impact parameter of the collision. TRENTo includes also the effects of fluctuations in the positions of the colliding nucleons, as well as in the magnitude of nucleon-nucleon interactions. These effects are tuned following the comprehensive phenomenological applications of Refs. [13, 14]. In each event I evaluate R according to Eq. (5). To express my results as function of quantities that are measurable, I use the effective hydrodynamic framework of Refs. [15, 16] to convert the relative variation of R into a reasonable approximation of the relative variation of \bar{p}_t as follows:

$$\frac{\bar{p}_t}{\langle \bar{p}_t \rangle} - 1 = -3c_s^2 \left(\frac{R}{\langle R \rangle} - 1 \right), \quad (6)$$

¹ I always refer to a 2+1-dimensional hydrodynamic expansion in the transverse plane. At ultrarelativistic energies, one can treat the quark-gluon plasma as invariant under longitudinal boosts [8], so that one needs to solve the dynamics only in the longitudinal slice at $z = 0$, where 0 corresponds to the interaction point of two nuclei.

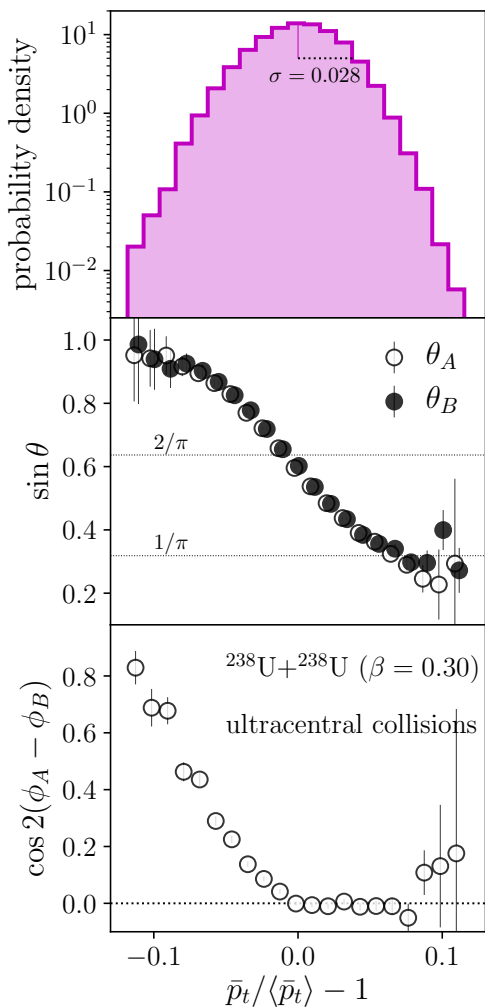


FIG. 3. Effect of sorting a batch of ultracentral U+U collisions according to their \bar{p}_t . In the uppermost panel, I show the distribution of \bar{p}_t around its average. In each bin of the histogram, I evaluate the average of the sine of the polar angles of the colliding nuclei (middle), and the average alignment between the azimuthal angles of the nuclei (lowermost panel), quantified by $\cos 2(\phi_A - \phi_B)$.

where angular brackets denote statistical averages in the multiplicity class, and I recall that \bar{p}_t is the average transverse momentum in *one* event. The speed of sound of the quark-gluon plasma, c_s^2 , appears in the equation as it tells us how an increase in temperature translates into an increase in pressure in the medium. The analysis of Ref. [15], indicates that $c_s^2 \approx 0.25$ at LHC energies, and that $c_s^2 \approx 0.19$ at RHIC energies.

I shall focus on $^{238}\text{U}+^{238}\text{U}$ collisions with shape parameters given in Tab. I. I simulate 25×10^6 collisions, and I select a bunch of events belonging to a narrow interval in the high-entropy tail. These events correspond experimentally to collisions belonging to the high-multiplicity tail. More specifically, I select events in the 0.25-0.50% multiplicity class.

Let me start by showing the dispersion of \bar{p}_t around its average value in the upper panel of Fig. 3. The histogram has a standard deviation of about 0.03. Model calculations of the distribution of \bar{p}_t in collisions of spherical ^{208}Pb nuclei at LHC energy have a standard deviation of order 0.02 [11]. The enhancement of fluctuations is mostly due to the fact the TRENTo model tuned to RHIC energy has larger fluctuations [14], but there is also a non-negligible contribution coming from the nonzero value of β , which enhances the fluctuations of transverse radius in U+U events. Note that the distribution is visibly skewed, as the tail on the left possess larger values of probability than the tail on the right. This is a direct consequence of the deformed nuclear shapes.

Moving on to the middle panel of Fig. 3, for each bin of the previous histogram I plot the values of $\sin \theta$ as function of \bar{p}_t for both nuclei. Note that the sine grows very close to unity at low \bar{p}_t . This indicates that, by selecting events in the low- \bar{p}_t tail, one selects events where $\theta_A = \theta_B = \pi/2$, confirming our expectations. Note that at large \bar{p}_t the sine flattens around $1/\pi$, which corresponds to the average value of the sine function in the interval $[0, \pi/2]$. This implies in particular that collisions with very large \bar{p}_t do not quite correspond to tip-tip events where $\theta_A = \theta_B = 0$. Closer investigation reveals that this has a simple explanation. The large- \bar{p}_t tail efficiently selects events with large impact parameter, rather than tip-tip configurations.

Finally, in the lower panel of Fig. 3 I compute the alignment of the two nuclei in the azimuthal plane by evaluating $\cos 2(\phi_A - \phi_B)$. At average and large transverse momentum, the correlator is consistent with zero, and the azimuthal angles are uncorrelated. Remarkably enough, there is a sudden increase in the alignment of the nuclei as one moves to lower \bar{p}_t values. The correlator gets close to 0.9, which implies almost perfect alignment between azimuthal angles.

In summary, this exercise proves the validity of the conjecture, motivated by the dimensional analysis, that the low- \bar{p}_t tail of ultracentral events is contained by fully overlapping body-body collisions. I point out now the nontrivial, observable consequence of this result.

REVEALING NUCLEAR DEFORMATION

Suppose that the medium created in a nucleus-nucleus collision is asymmetric in the transverse plane, e.g., its transverse size along the x direction, R_x , is larger than its size along y , R_y . This occurs naturally, for instance, in a noncentral collisions where x is the direction of the impact parameter. Spatial asymmetry yields an imbalance of pressure gradients [17], that are stronger along x than along y . Equation (1) and the dimensional analysis

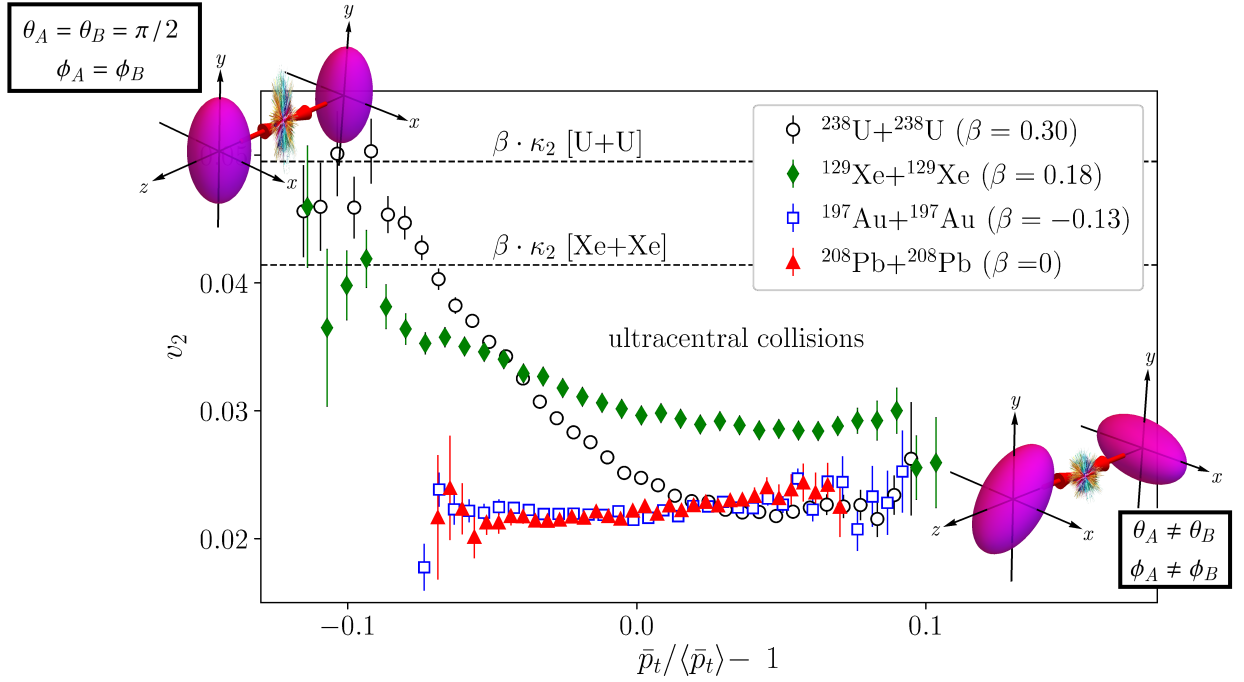


FIG. 4. Elliptic flow as function of the average transverse momentum in ultracentral collisions of ^{238}U , ^{208}Pb , ^{197}Au and ^{129}Xe nuclei. The cartoons illustrate the expected orientations of the colliding nuclei in the tails of the \bar{p}_t distribution.

yield, then, an imbalance of force in the fluid [18]

$$\frac{1}{R_x} > \frac{1}{R_y} \Rightarrow F_x > F_y, \quad (7)$$

so that more momentum is built in the fluid along the x direction than along the y direction. This phenomenon is called *elliptic flow*. Experimentally, it manifests as an angular imbalance in the amount of momentum carried by the produced particles, corresponding to a pronounced $\cos(2\phi)$ modulation of the azimuthal particle spectrum:

$$\frac{dN}{d\phi} \propto 1 + 2v_2 \cos(2\phi), \quad (8)$$

where v_2 quantifies the magnitude of elliptic flow.

Let us go, then, back to Fig. 2. While tip-tip collisions produce a quark-gluon plasma with a circular background geometry, body-body collisions create systems with a manifest background elliptical asymmetry, due to the deformation of the colliding bodies. Equation (7) implies, then, that the largest elliptic flow is achieved in fully-overlapping body-body collisions. Now combine this argument with the previous observation that fully-overlapping body-body collisions are those presenting abnormally small values of \bar{p}_t . Nuclear deformation yields, then, an enhancement of elliptic flow in the low- \bar{p}_t tail of ultracentral collisions.

I verify this statement using the TRENTo model. I shall not, though, compute elliptic flow by means of full hydrodynamic simulations. I use the fact that elliptic

flow is a response to the elliptic anisotropy of the initial density profile. The *eccentricity* of the medium at the beginning of hydrodynamics, denoted by ε_2 , is the second-order Fourier harmonic of the entropy profile [19]:

$$\varepsilon_2 = \frac{\int_{\mathbf{x}} \mathbf{x}^2 s(\mathbf{x})}{\int_{\mathbf{x}} |\mathbf{x}|^2 s(|\mathbf{x}|)} \quad (9)$$

where \mathbf{x}^2 is here in complex notation, $\mathbf{x}^2 = (x + iy)^2$. Hydrodynamic simulations [20] show that elliptic flow is essentially a linear response to the initial eccentricity, and that the following relation holds to a very good approximation in central nucleus-nucleus collisions:

$$v_2 = \kappa_2 \varepsilon_2. \quad (10)$$

κ_2 is a response coefficient that depends on the properties of the medium, such as its viscosity. The value of κ_2 has been determined at both RHIC and LHC energies, by comparing the eccentricity provided by the TRENTo model with data on v_2 . This knowledge allows me to estimate elliptic flow without running hydrodynamics.

Let me discuss first U+U collisions. Within the same batch of ultracentral events used in Fig. 3, I calculate ε_2 as function of \bar{p}_t , and I rescale it by a factor $\kappa_2 = 0.17$ [14] to obtain the final-state elliptic flow. The result is shown as empty circles in Fig. 4. The intuitive prediction is perfectly confirmed. Elliptic flow is strongly enhanced in the low- \bar{p}_t region, because one approaches the limit of fully-overlapping body-body collisions. Note that the value of elliptic flow saturates around a value that is close

species	a [fm]	R [fm]	β
^{238}U [22]	0.60	6.80	0.3
^{208}Pb [23]	0.55	6.62	0
^{197}Au [23]	0.53	6.40	-0.13 [24]
^{129}Xe [25]	0.59	5.40	0.18 [25]
^{96}Ru [26]	0.46	5.08	0.16 [27]
^{96}Zr [26]	0.46	5.02	0.08 [27]

TABLE I. Parameters used in Eq. (2) for different species.

to $\beta\kappa_2$, which implies $\varepsilon_2 \approx \beta$. In such collisions, then, the elliptic anisotropy of the system is essentially determined by the value of β , i.e., by the shape of the nuclei.

In Fig. 4 I present as well results from TRENTo simulations of other systems, whose density parameters are listed in Tab. I. Results similar to those observed in U+U collisions are obtained for collisions of prolate ^{129}Xe nuclei ($\kappa_2 = 0.23$ [13]). For collisions of spherical ^{208}Pb nuclei ($\kappa_2 = 0.24$ [21]) and of mildly-oblate ^{197}Au nuclei ($\kappa_2 = 0.16$ [14]), there is instead no visible effect. I appreciate a slight rise of v_2 with \bar{p}_t for Pb+Pb collisions. This occurs because large- \bar{p}_t events probe large impact parameters, and large impact parameters generate a v_2 by construction. The same trend is observed in Au+Au collisions. It is interesting to note that, for collisions of oblate nuclei ($\beta < 0$), the enhancement of elliptic flow should occur in the large- \bar{p}_t tail. However, there is very little hint of such an effect in my results implementing $\beta = -0.13$. The presence of a sizable impact parameter at large \bar{p}_t smears the effect due to the oblate shapes.

For completeness, I check the behavior of the third harmonic, v_3 [28], reflecting the triangular anisotropy of the initial condition, ε_3 [19]. Looking at ε_3 as function of \bar{p}_t , I find a null result. The resulting curve is flat in both U+U and Pb+Pb collisions.

Finally, I discuss the case of $^{96}\text{Zr}+^{96}\text{Zr}$ and $^{96}\text{Ru}+^{96}\text{Ru}$ collisions, performed in 2018 at RHIC. From a hydrodynamic point of view, these experiments are interesting because they create QGPs possessing the same hydrodynamic properties, i.e., the same value of κ_2 . The eccentricity, ε_2 , on the other hand, depends on the deformation of these species. The data-driven analysis of Ref. [27], indicates that $\beta = 0.08$ for ^{96}Zr , while $\beta = 0.16$ for ^{96}Ru . It is interesting to note the comprehensive model extrapolations of Ref. [24] seem to contradict this result, suggesting that ^{96}Ru is spherical while ^{96}Zr is deformed with $\beta \approx 0.2$. In my calculation I shall follow Ref. [27] (see Tab. I). I show my predictions for elliptic flow in Fig. 5. Since I do not know the values of κ_2 for these systems, I normalize the value of v_2 by the value it has in a small bin of $\bar{p}_t/\langle\bar{p}_t\rangle - 1$ centered at 0, a trick which allows to get rid of the constant κ_2 . The results shown in Fig. 5 should be compared directly with data. I notice two interesting features. First, one sees a distinct enhancement of elliptic flow for a value of β that is as small as 0.08.

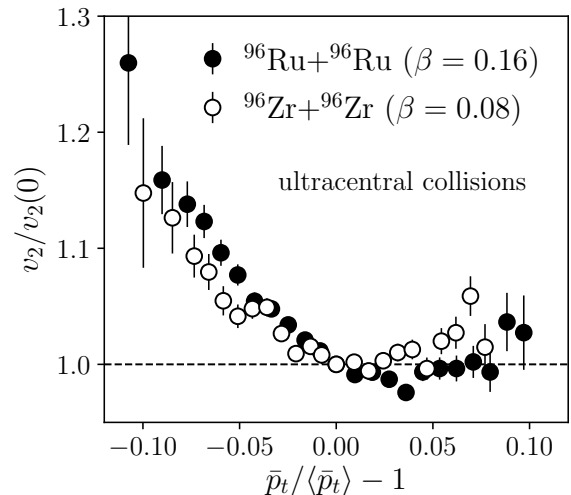


FIG. 5. Scaled elliptic flow as function of the average transverse momentum in ultracentral collisions of ^{96}Ru and ^{96}Zr nuclei.

Second, Ru+Ru systems are more enhanced. This difference originates solely in the larger value of β . If observed, it will allow to unambiguously determine which of these nuclei has largest deformation.

CONCLUSIONS

I introduced a method for experimental analyses of relativistic nuclear collisions which allows to select body-body ultracentral events. In such events, the elliptic flow of outgoing hadrons becomes a direct measure of the deformation of the colliding species.

The scaled elliptic flow of low- \bar{p}_t ultracentral collisions shown in Fig. 5 is so sensitive to the value of β that one could simply look at its behavior to know whether nuclei are prolate, even for small deformations. This is not possible in current analyses, where one averages over orientations, and the effect of deformation can only be inferred by comparing results to those of Pb+Pb data, and only if β is large enough.

My method, if confirmed in experiments, should allow to perform new experimental verification of ab-initio calculations of nuclear structure. It should be combined, in particular, with the great versatility of RHIC to put new constraints on the quadrupole deformation of potentially a very large number of stable nuclides.

ACKNOWLEDGMENTS

I acknowledge the kind hospitality of the physics department of the Brookhaven National Laboratory where most of this manuscript was written.

-
- [1] W. Busza, K. Rajagopal and W. van der Schee, *Ann. Rev. Nucl. Part. Sci.* **68**, 339 (2018) doi:10.1146/annurev-nucl-101917-020852 [arXiv:1802.04801 [hep-ph]].
- [2] M. Luzum, *J. Phys. G* **38**, 124026 (2011) doi:10.1088/0954-3899/38/12/124026 [arXiv:1107.0592 [nucl-th]].
- [3] P. Romatschke and U. Romatschke, doi:10.1017/9781108651998 arXiv:1712.05815 [nucl-th].
- [4] L. Adamczyk *et al.* [STAR Collaboration], *Phys. Rev. Lett.* **115**, no. 22, 222301 (2015) doi:10.1103/PhysRevLett.115.222301 [arXiv:1505.07812 [nucl-ex]].
- [5] A. M. Sirunyan *et al.* [CMS Collaboration], *Phys. Rev. C* **100**, no. 4, 044902 (2019) doi:10.1103/PhysRevC.100.044902 [arXiv:1901.07997 [hep-ex]].
- [6] S. Acharya *et al.* [ALICE Collaboration], *Phys. Lett. B* **784**, 82 (2018) doi:10.1016/j.physletb.2018.06.059 [arXiv:1805.01832 [nucl-ex]].
- [7] B. Schenke, P. Tribedy and R. Venugopalan, *Phys. Rev. C* **89**, no. 6, 064908 (2014) doi:10.1103/PhysRevC.89.064908 [arXiv:1403.2232 [nucl-th]].
- [8] J. D. Bjorken, *Phys. Rev. D* **27**, 140 (1983). doi:10.1103/PhysRevD.27.140
- [9] W. Broniowski, M. Chojnacki and L. Obara, *Phys. Rev. C* **80**, 051902 (2009) doi:10.1103/PhysRevC.80.051902 [arXiv:0907.3216 [nucl-th]].
- [10] A. Mazeliauskas and D. Teaney, *Phys. Rev. C* **93**, no. 2, 024913 (2016) doi:10.1103/PhysRevC.93.024913 [arXiv:1509.07492 [nucl-th]].
- [11] P. Bozek and W. Broniowski, *Phys. Rev. C* **96**, no. 1, 014904 (2017) doi:10.1103/PhysRevC.96.014904 [arXiv:1701.09105 [nucl-th]].
- [12] J. S. Moreland, J. E. Bernhard and S. A. Bass, *Phys. Rev. C* **92**, no. 1, 011901 (2015) doi:10.1103/PhysRevC.92.011901 [arXiv:1412.4708 [nucl-th]].
- [13] G. Giacalone, J. Noronha-Hostler, M. Luzum and J. Y. Ollitrault, *Phys. Rev. C* **97**, no. 3, 034904 (2018) doi:10.1103/PhysRevC.97.034904 [arXiv:1711.08499 [nucl-th]].
- [14] G. Giacalone, *Phys. Rev. C* **99**, no. 2, 024910 (2019) doi:10.1103/PhysRevC.99.024910 [arXiv:1811.03959 [nucl-th]].
- [15] F. G. Gardim, G. Giacalone, M. Luzum and J. Y. Ollitrault, arXiv:1908.09728 [nucl-th].
- [16] F. G. Gardim, G. Giacalone and J. Y. Ollitrault, arXiv:1909.11609 [nucl-th].
- [17] J. Y. Ollitrault, *Phys. Rev. D* **46**, 229 (1992). doi:10.1103/PhysRevD.46.229
- [18] J. Y. Ollitrault, *Eur. J. Phys.* **29**, 275 (2008) doi:10.1088/0143-0807/29/2/010 [arXiv:0708.2433 [nucl-th]].
- [19] D. Teaney and L. Yan, *Phys. Rev. C* **83**, 064904 (2011) doi:10.1103/PhysRevC.83.064904 [arXiv:1010.1876 [nucl-th]].
- [20] H. Niemi, K. J. Eskola and R. Paatelainen, *Phys. Rev. C* **93**, no. 2, 024907 (2016) doi:10.1103/PhysRevC.93.024907 [arXiv:1505.02677 [hep-ph]].
- [21] G. Giacalone, P. Guerrero-Rodriguez, M. Luzum, C. Marquet and J. Y. Ollitrault, *Phys. Rev. C* **100**, no. 2, 024905 (2019) doi:10.1103/PhysRevC.100.024905 [arXiv:1902.07168 [nucl-th]].
- [22] Q. Y. Shou, Y. G. Ma, P. Sorensen, A. H. Tang, F. Videbk and H. Wang, *Phys. Lett. B* **749**, 215 (2015) doi:10.1016/j.physletb.2015.07.078 [arXiv:1409.8375 [nucl-th]].
- [23] H. De Vries, C. W. De Jager and C. De Vries, *Atom. Data Nucl. Data Tabl.* **36**, 495 (1987). doi:10.1016/0092-640X(87)90013-1
- [24] P. Möller, A. J. Sierk, T. Ichikawa and H. Sagawa, *Atom. Data Nucl. Data Tabl.* **109-110**, 1 (2016) doi:10.1016/j.adt.2015.10.002 [arXiv:1508.06294 [nucl-th]].
- [25] S. Acharya *et al.* [ALICE Collaboration], *Phys. Lett. B* **790**, 35 (2019) doi:10.1016/j.physletb.2018.12.048 [arXiv:1805.04432 [nucl-ex]].
- [26] W. T. Deng, X. G. Huang, G. L. Ma and G. Wang, *Phys. Rev. C* **94**, 041901 (2016) doi:10.1103/PhysRevC.94.041901 [arXiv:1607.04697 [nucl-th]].
- [27] S. Raman, C. W. G. Nestor, Jr and P. Tikkannen, *Atom. Data Nucl. Data Tabl.* **78**, 1 (2001). doi:10.1006/adnd.2001.0858
- [28] B. Alver and G. Roland, *Phys. Rev. C* **81**, 054905 (2010) Erratum: [*Phys. Rev. C* **82**, 039903 (2010)] doi:10.1103/PhysRevC.82.039903, 10.1103/PhysRevC.81.054905 [arXiv:1003.0194 [nucl-th]].